Available online at www.sciencedirect.com
ScienceDirect
Applied Catalysis B: Environmental 79 (2008) 208–215
APPLIED CATALYSIS B: ENVIRONMENTAL
www.elsevier.com/locate/apcatb

# Zn-doped $TiO_2$ nanoparticles with high photocatalytic activity synthesized by hydrogen–oxygen diffusion flame

Yin Zhao [a,b], Chunzhong Li [a,*], Xiuhong Liu [a], Feng Gu [a], H.L. Du [c], Liyi Shi [b]

[a] *Key Laboratory for Ultrafine Materials of Ministry of Education, School of Materials Science and Engineering, East China University of Science & Technology, Shanghai 200237, China*
[b] *Research Center of Nanoscience & Nanotechnology of Shanghai University, Shanghai University, Shanghai 200436, China*
[c] *Advanced Materials Research Institute, Northumbria University, Newcastle Upon Tyne NE1 8ST, United Kingdom*

Received 4 January 2007; received in revised form 17 September 2007; accepted 25 September 2007
Available online 9 October 2007

**Abstract**

Zn-doped $TiO_2$ nanoparticles with high photocatalytic activity were synthesized by the hydrogen–oxygen diffusion flame method and the photocatalytic degradation mechanism of rhodamine B dye under visible light irradiation were elaborated. The Zn dopants presented in the form of small ZnO nuclei dispersing randomly on the surface of anatase $TiO_2$ nanoparticles. It is found that the photosensitized degradation activity can be enhanced by doping an appropriate amount of Zn. The improved activity by Zn doping can be attributed to the appropriate energetic position between ZnO and the excited state of dye, which enhanced the electron injection into the conduction band of $TiO_2$ by capturing electron, subsequently promoted the formation of reactive oxygen species. Hence, the enhanced photodegradation of dyes under visible irradiation can be realized.


*Keywords:* Titanium dioxide; Photocatalytic; Nanoparticles; Zinc oxide; Dopant; Gas flame combustion; Surface oxygen vacancies

## 1. Introduction

The applications of semiconductor $TiO_2$ in the photocatalytic oxidation of many undesirable environmental contaminants and the photoelectrochemical conversion of solar energy have been extensively studied owing to its high photostability, nontoxicity, low cost and availability [1–4]. Recently, $TiO_2$ irradiated by UV light has become the benchmark photocatalyst for degrading environmental contaminants as documented in literature [5]. However, the major drawback of $TiO_2$ lies in the fact that the absorbance of only a narrow portion of solar spectra in the UV region due to the large band gap of $TiO_2$. To overcome this limitation, numerous studies have been recently performed [6–8]. Among these, the photosensitized degradation process has the advantage through harvesting the maximum of solar energy by utilizing visible light for degradation of the dye containing wastewaters, which is one of the major environmental contaminations in textile and photographic industries [9,10]. In the photosensitized degradation process, the dyes act as both photosensitizer and degraded substrates. The dyes are activated into their excited states with injecting an electron into the conduction band of $TiO_2$. The ejected electron reacts with adsorbed oxidants (usually $O_2$) to produce active oxygen radicals (e.g., $O_2^{\bullet -}$, $^{\bullet}OOH$, $^{\bullet}OH$), which subsequently degrade or mineralize the dyes [11–14]. The self-sensitization of dye is its own oxidative transformation by the indirect formation of active oxygen radicals. The existence of $TiO_2$ is a prerequisite, which plays an important role of electron carriers to electron acceptors adsorbed on the particles.

In the process of photosensitized degradation of dyes, the conditions of ejected electron can greatly affect the interfacial charge transfer processes which strongly depend on the surface characteristics of $TiO_2$ particles and the motilities and lifetime of charge carriers. The modification of $TiO_2$ by doping metal ions and coupling other semiconductors can significantly influence the processes of photosensitized degradation. It was reported [15–18] that $TiO_2$ doped with Pt, Pd, Au, Ag and Fe can effectively suppress the electron–hole recombination by acting as an electron and/or hole traps. Marci et al. [19] found that Zn can considerably enhance the photocatalytic perfor-

* Corresponding author. Tel.: +86 21 64250949; fax: +86 21 64250624.
*E-mail address:* czli@ecust.edu.cn (C. Li).

0926-3373/$ – see front matter © 2007 Elsevier B.V. All rights reserved.
doi:10.1016/j.apcatb.2007.09.044

mance of $TiO_2$ under UV irradiation, which was attributed to the increase in the separation rate of photoinduced charge due to the difference in the energy band position. The dynamic processes of photoinduced charges are affected by the oxygen vacancies, which can be determined sometimes on the metal ions adoped in the surface of $TiO_2$ nanoparticles [20–23]. However, almost no research has been carried out to investigate the influence of modified $TiO_2$ on the photosensitized degradation of dyes under visible light irradiation. Also, it is of great importance to study the effects of Zn doping in $TiO_2$ on the electron transfer and the Zn modification mechanisms relating to the surface oxygen vacancies in order to find an effective method to enhance the catalytic activity.

Though several approaches such as sol–gel method [24] and liquid-phase precipitation [19] are widely used to obtain Zn-doped $TiO_2$, the flame synthesis can provide well-mixed precursors at an atomic level and desired size range within narrow size distribution without an additional treatment, thus making it feasible to process chemically homogenous, uniform and well-dispersed powders [25,26]. In this paper, Zn-doped $TiO_2$ particles with high photocatalytic activity under visible light irradiation were synthesized by the flame method. The effects of Zn distribution on the particle surface, surface oxygen vacancies and the energetic positions among ZnO, $TiO_2$ and excited state of the dyes on the processes of photosensitized dye-degradation were investigated.

## 2. Experimental

Zn-doped $TiO_2$ nanoparticles were prepared by feeding the relevant volatilized precursors into modified hydrogen–oxygen co-flow diffusion flame reactor (shown in Fig. 1), which was designed to obtain particles with uniform and well-dispersion characteristics, facilitated by introducing the diluted gas into centre tube [27,28]. The reactor consisted of three concentric stainless-steel tubes with inner diameters of 3.0 mm, 6.0 mm, and 10.0 mm, respectively. $TiCl_4$ was carried by passing nitrogen through a gas washing bottle containing $TiCl_4$ at 90 °C. The $TiCl_4$-saturated nitrogen stream and clean air (2.1 L/min) were introduced into central tube of the flame reactor along with 1.5 L/min hydrogen (inner annulus) and 0.8 L/min of oxygen (outer annulus) resulting in a stabilized diffusion flame. Zinc acetylacetonate, the dopant precursor, was introduced into the central tube by passing nitrogen over sublimation unit filled with zinc acetylacetonate. The contents of dopant were adjusted by the flow rate of carrier gas and the evaporation temperature, which was controlled between 90 and 120 °C. The delivery tube and burner were kept at 200 °C to prevent the condensation of zinc acetylacetonate. All gases were delivered from cylinders and their flow rates were monitored by rotameters. The as-prepared $TiO_2$ products were collected on the filter with the aid of a vacuum pump. Table 1 gives the experimental conditions and properties of Zn-doped $TiO_2$ nanoparticles.

The photosensitized activity of Zn-doped $TiO_2$ was measured in terms of the decolourization of an active organic dye RhB. The catalysts were dispersed in a 50 mL of standard RhB aqueous solution (20 mg/L), using 70 mL capacity of quartz tube. The weight of the photocatalyst used in each experiment was 0.05 g. Visible lights (>400 nm) were obtained by a 1000 W linear halogen lamp with glass filters and the distance between the light and the reaction tube was 10 cm. Prior to reaction, the catalysts were agitated for 30 min in RhB solution in the absence of lights in order to attain the stabilized adsorption on the catalyst surface. After a given irradiation time, the samples were withdrawn for subsequent analysis with a UV–vis spectrophotometer (Shanghai 760).

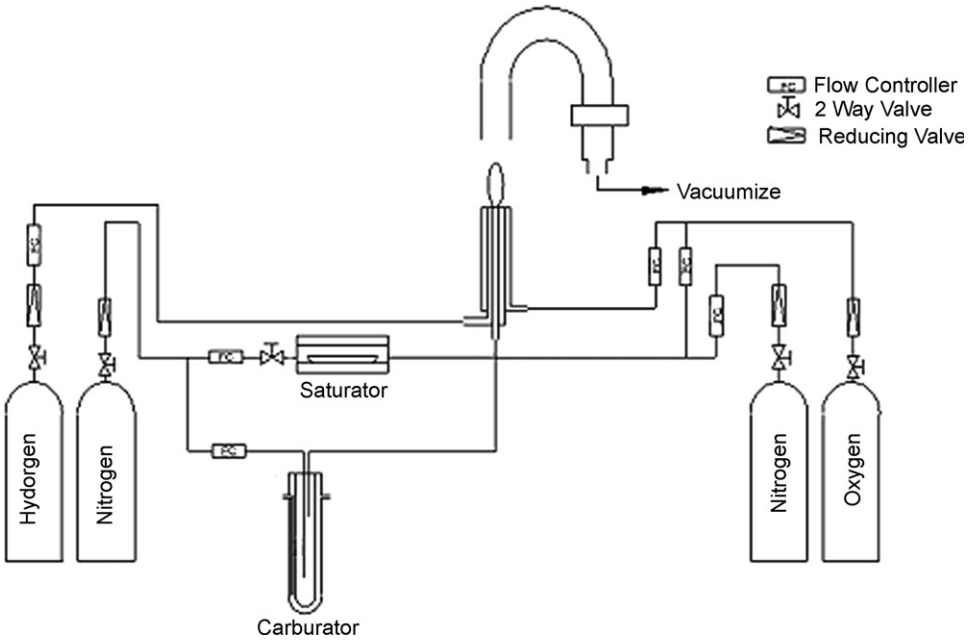


Fig. 1. Schematics of experimental apparatus.

Table 1
Summary of experimental conditions and characteristics of the resultant $TiO_2$ nanoparticles

| Sample | Experimental parameters[a] | | Particle size, $d_{XRD}$ (nm) | Phase content (anatase wt.%) |
|---|---|---|---|---|
| | Ti (mL/min) | Zn (mL/min)/temp (°C) | | |
| A | 0.6 | 0 | 12.7 | 100 |
| B | 0.6 | 0.05/90 | 13.3 | 100 |
| C | 0.6 | 0.3/120 | 13.1 | 100 |
| D | 0.6 | 0.4/120 | 12.9 | 100 |

[a] Ti and Zn represent the flow of nitrogen introducing the titanium precursor and zinc acetylacetonate, respectively. Temp represents the temperature of sublimation unit.

X-ray diffraction (XRD) patterns of the samples were collected in the range of 20–80° (2$\theta$) using a Rigaku D/max 2550 diffractometer (Cu Kα radiation, λ = 1.5406 Å), operated at 40 kV and 100 mA. The crystallite size was estimated by applying the Scherrer equation to the full width at half-maximum (fwhm) of the (1 0 1) peak of anatase, with *R*-silicon (99.9999%) as a standard for the instrumental line broading. Transmission electron micrograph images were taken with a JEM-100CXII transmission electron microscope (TEM). Elemental analysis was carried out by inductively coupled plasma-atomic emission spectroscopy (ICP-AES) at TJAIRIS 1000. X-ray photoelectron spectroscopy (XPS) spectra were recorded by a PHI 5000C ESCA spectrometer using Mg Kα radiation ($h\nu$ = 1253.6 eV). The pressure of the analyzer chamber was maintained at $5 \times 10^{-8}$ Pa. The shift of the binding energy due to relative surface charging was corrected using the C 1s level at 284.6 eV as an internal standard. The experimental spectra were resolved into Lorentzian–Gaussian components after subtraction of a linear background, using a nonlinear least squares fitting route. The quantitative analysis of the sample was performed using the route software of the XPS instrument with appropriate sensitivity factors. Diffuse reflectance spectra (DRS) were obtained for the dry-pressed disk samples using a Scan UV–vis–NIR spectrophotometer (Varian, Cary 500) equipped with an integrating sphere assembly, using $BaSO_4$ as reflectance sample. The spectra were recorded at room temperature in air, in the range of 200–800 nm.

## 3. Results and discussion

### 3.1. Morphology and microstructure

XRD patterns of $TiO_2$ samples with and without Zn doping are shown in Fig. 2. All samples exhibit the similar patterns assigned well to the anatase crystalline phase of $TiO_2$. Due to the low Zn content, the possible impurities such as zinc oxide were not detected. The primary particle sizes of the samples determined by the peak broadening method were 12.7–13.3 nm (Table 1). The results indicate that Zn doping did not affect the particle size of $TiO_2$ nanoparticles. TEM images illustrated in Fig. 3 demonstrate that $TiO_2$ nanoparticles were ultrafine and dispersed homogeneously. According to the TEM photographs, the particle size was about 14 nm, consistent with the XRD results.

The XPS spectra of Ti 2p of pure and Zn-doped $TiO_2$ samples depicted in Fig. 4 show two peaks at 458.1 eV and 463.8 eV, which can be assigned to the core levels of $Ti^{4+}$ $2p_{3/2}$ and $Ti^{4+}$ $2p_{1/2}$, respectively [29]. Compared with samples A and B, Ti peaks of sample C shifted to higher binding energy. But it is possible due to the disturbance of the noisy peak, the shift of sample D is not obvious. This shift can prove the existence of Ti with lower valence. The formation of Ti with lower valence can be attributed to the existence of lots of oxygen vacancies in the nanoparticles after doping Zn. XPS spectra of Zn 2p region are given in Fig. 5. Zn ($2p_{3/2,\ 1/2}$) doublet was observed at 1021.0 eV and 1044.2 eV, indicating Zn in 2+ state bonding with oxygen. The content of Zn derived from XPS was larger than that of ICP-AES analysis (Table 2). It is apparent that XPS analysis reflects the surface composition condition, while ICP-AES results give the average composition condition of the samples. Therefore, it can be concluded that most of $Zn^{2+}$ ions resided on the surface of the $TiO_2$ particles. The large difference between the ionic radii of $Zn^{2+}$ (0.88 Å) and $Ti^{4+}$ (0.745 Å) makes it difficult for $Zn^{2+}$ to substitute $Ti^{4+}$. If a $Zn^{2+}$ ion replaces a $Ti^{4+}$ site, the $TiO_2$ host lattice would have to deform, which is energetically unfavourable. On the other hand, the differences in chemical properties between $Zn^{2+}$ and $Ti^{4+}$ would not favour the substitution of $Ti^{4+}$ by $Zn^{2+}$. Therefore, it can be confirmed that Zn ions possibly exist mainly in the form of ZnO clusters and dispersed on $TiO_2$ crystallite surfaces. The XPS spectra of O 1s core level of pure and Zn-doped $TiO_2$

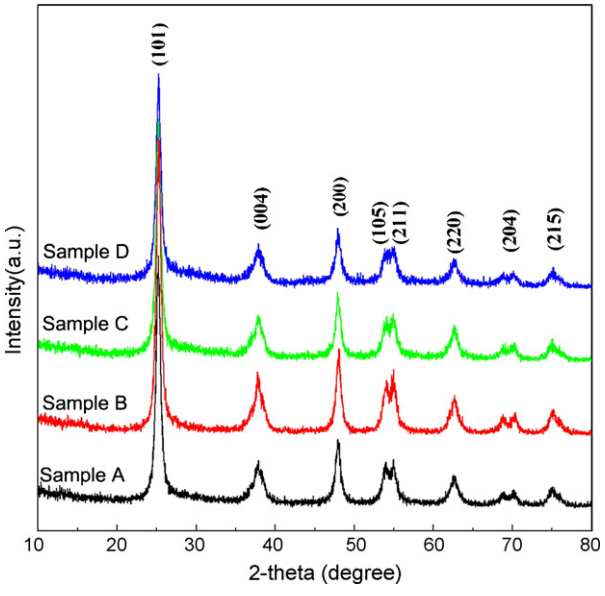


Fig. 2. XRD patterns of pure and Zn-doped $TiO_2$ samples.

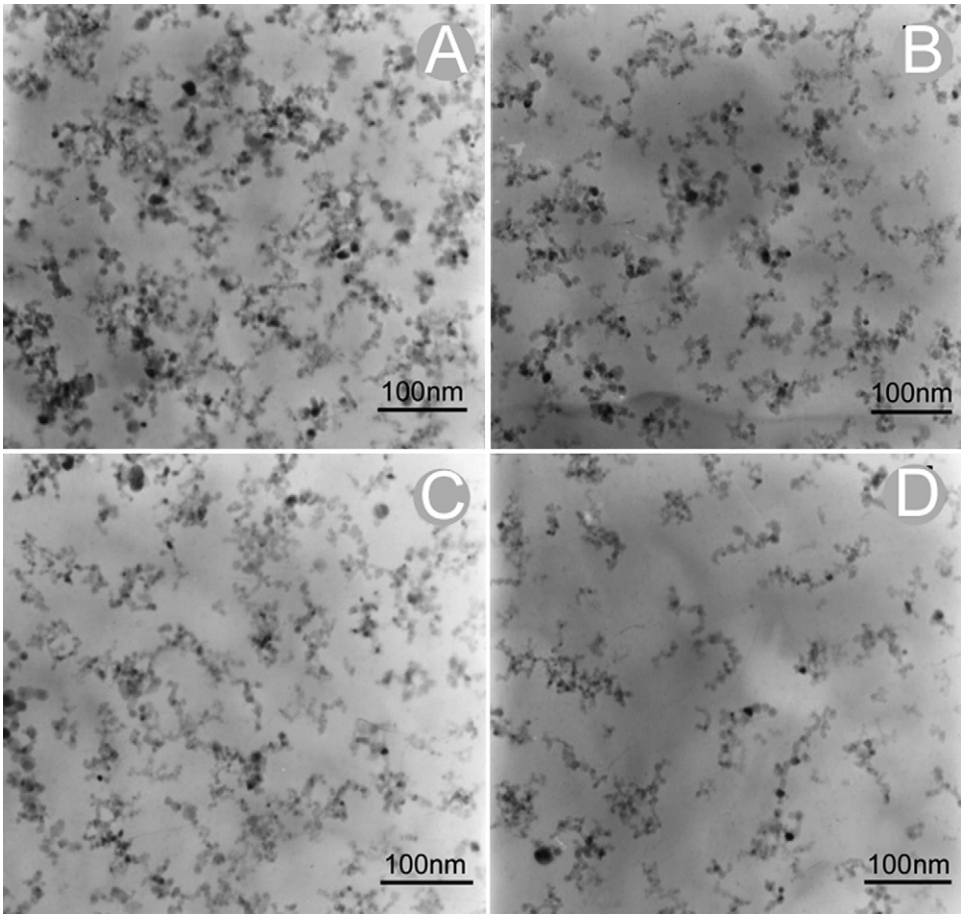


Fig. 3. TEM images of pure and Zn-doped $TiO_2$ samples.

samples are asymmetric (Fig. 6A), indicating that there are at least two kinds of chemical states. After curve fitting, besides the peak corresponding to the lattice oxygen of $TiO_2$ ($O_L$), the other peak at higher binding energy can be identified (Fig. 6B) [30]. This peak should be attributed to the surface species such as Ti–OH and Ti–O–O resulting from the chemisorbed water ($O_H$) [31]. The fitting results listed in Table 2 give the corresponding XPS data, atomic number ratio and relative content of surface oxygen vacancies. As seen from Table 2, the percentage of surface oxygen vacancies is 19.1 for pure $TiO_2$, while 25.5 for $TiO_2$ nanoparticles with high level of Zn doping (sample D), indicating that the content of surface oxygen vacancies is enhanced by doping Zn.

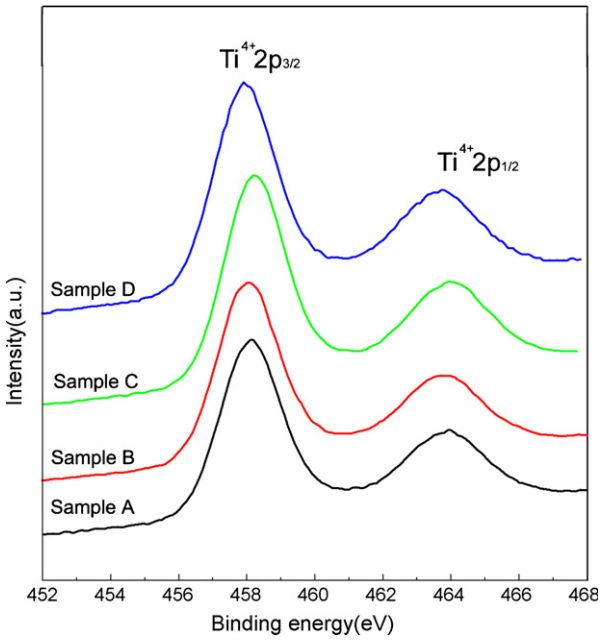


Fig. 4. Ti 2p XPS core level spectra of pure and Zn-doped $TiO_2$ samples.

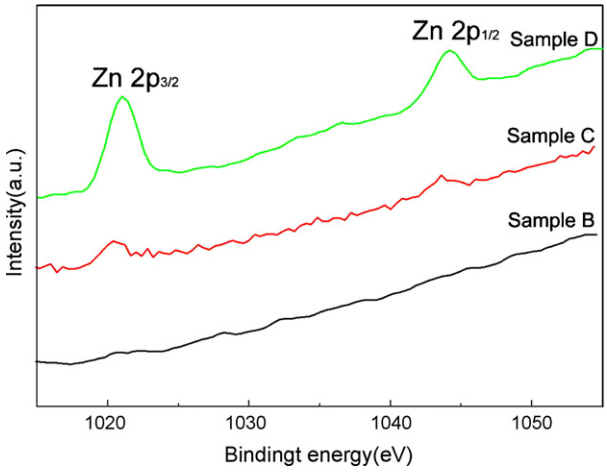


Fig. 5. XPS spectra of Zn 2p for Zn-doped $TiO_2$ samples.

Table 2
Binding energies (eV) of Ti 2p, O 1s and Zn 2p, Zn/Ti the molar ratios (mol%) and the content of surface oxygen vacancies (SOV)

| Sample | Binding energy (eV) | | | $x/TiO_x$ | SOV content/%[a] | Zn/Ti (XPS) | Zn/Ti (ICP) |
|---|---|---|---|---|---|---|---|
| | Ti $2p_{3/2}$ | $O_L$ 1s (Ti–O) | $O_H$ 1s (O–H) | | | | |
| A | 458.1 | 529.3 | 531.8 | 1.62 | 19.1 | – | – |
| B | 458.0 | 529.2 | 531.6 | 1.63 | 18.5 | 0.37 | 0.014 |
| C | 458.1 | 529.3 | 531.6 | 1.55 | 22.4 | 1.34 | 0.85 |
| D | 457.9 | 529.1 | 531.7 | 1.49 | 25.5 | 4.32 | 2.18 |

[a] SOV represent the surface oxygen vacancies (SOV) of $TiO_2$. The SOV can be estimated by using the equation [24]: SOV = $(2 - x)/2 \times 100\%$, where $x$ is the molar ratios of $O_L$ and Ti.

### 3.2. UV–vis absorption analysis and photocatalytic activity

Fig. 7 shows the UV–vis absorption spectra of the pure and Zn-doped $TiO_2$ samples. By using the procedure given by Wang et al. [32], the absorption edge appears red-shift and the band and gap decreases with increasing Zn content. According to the energy band structure of $TiO_2$, the optical absorption at the wavelength range of shorter than 400 nm is mainly attributed to the electron transitions from the valence band to conduction band (band-to-band transition, O 2p → Ti 3d), while the weak optical absorption at the wavelength range from 400 nm to 550 nm results from sub-band transitions closely related to the SOVs [33]. It can be found that the red-shift of absorption edge after doping Zn is in good agreement with XPS results about the SOVs. Therefore, the red-shift can be attributed to the increase in the SOV amount. In addition, as a dopant, ZnO can serve as a component in the composites, the interfacial coupling effect between ZnO and $TiO_2$ particles is also possibly cause the red-shift of the band gap.

The aqueous solution of RhB dye is fairly stable to visible radiation the absence of $TiO_2$ photocatalyst. However, the RhB can be degraded efficiently in RhB/$TiO_2$ aqueous dispersions under visible light irradiation at wavelengths of longer than 400 nm through a photosensitized path [12,13]. The UV–vis spectra changing upon time during the photodegradation of RhB in the pure and Zn-doped $TiO_2$ aqueous dispersions under visible light irradiation are shown in Fig. 8. The results show that the decrease of absorption maximum with a concomitant blue-shift to a certain extent for both pure and Zn-doped $TiO_2$ nanoparticles. The decrease of absorption maximum is due to the principal attack of $^{\bullet}OH$ radicals in the solution at the aromatic chromophore ring. The blue-shift of the absorption band is caused by the formation of a series of *N*-de-ethylated intermediates in a stepwise manner [11]. The competitive photodegradation reactions between the de-ethylation and cleavage of RhB chromophore ring structure occur in these

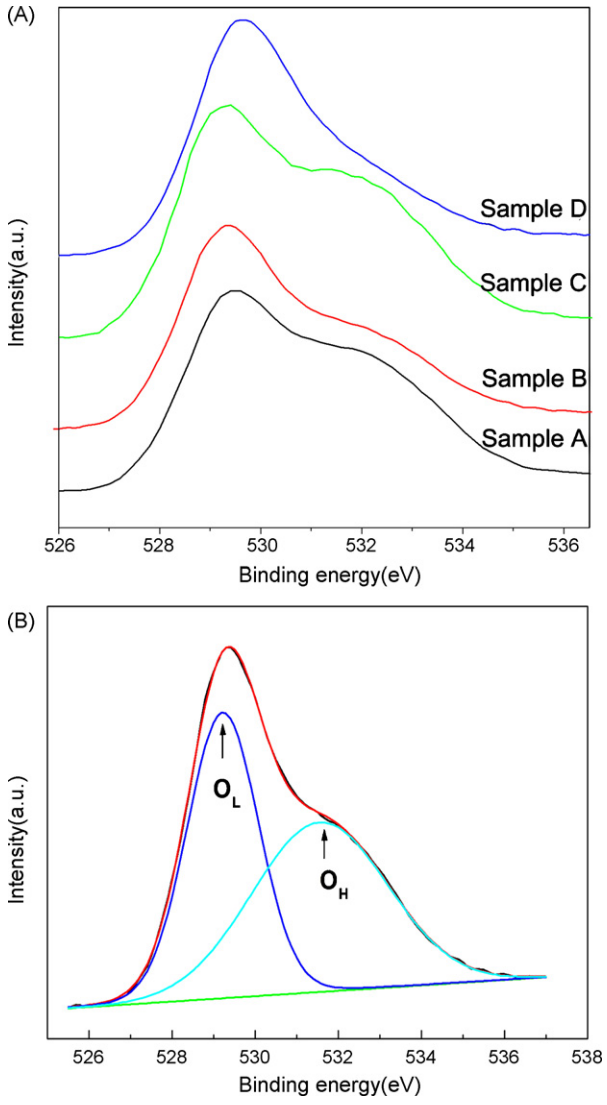


Fig. 6. (A) O 1s XPS core level spectra of pure and Zn-doped $TiO_2$ samples and (B) O 1s fitting results for sample B.

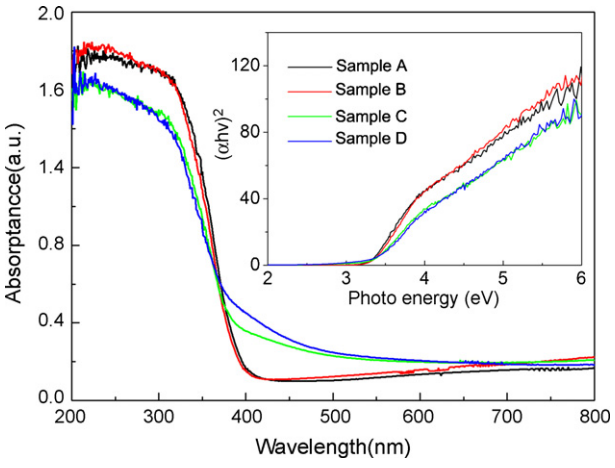


Fig. 7. UV–vis diffuse reflectance spectra of the pure and Zn-doped $TiO_2$ samples.

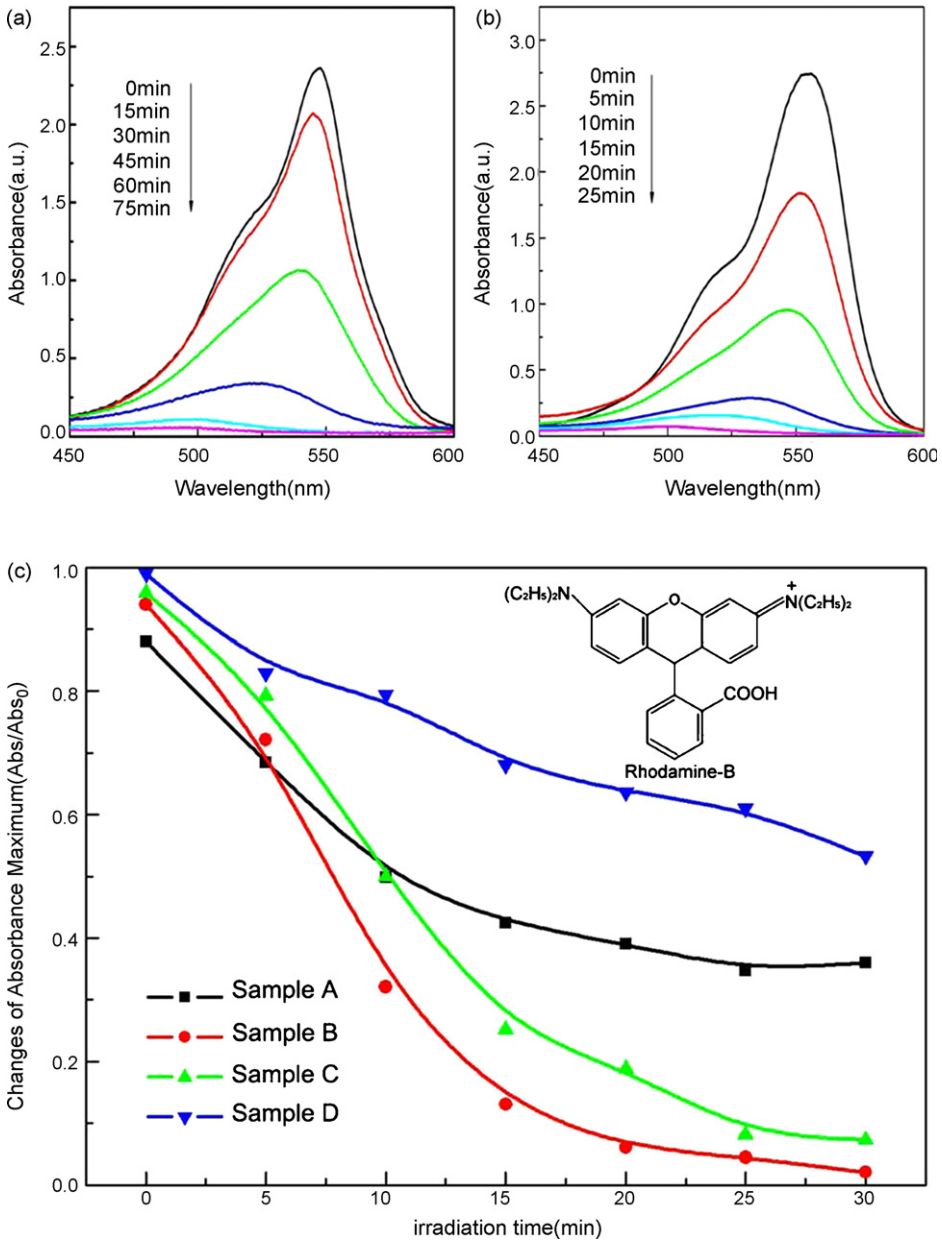


Fig. 8. UV–vis spectral changes of (A) RhB/pure $TiO_2$ system (sample A), (B) RhB/Zn-doped $TiO_2$ system (sample B) and (C) absorbance changes for pure and Zn-doped $TiO_2$ samples as a function of irradiation time (the $Abs_0$ and Abs represent the absorption of dye at initial and the given irradiation time, respectively). The inset shows the molecular structural of rhodamine B.

photocatalytic systems. The discoloration and mineralization of RhB can be ultimately take place under the synergistic reaction. Comparison of the absorbance changes in the major absorption band of RhB/$TiO_2$ and RhB/Zn-doped $TiO_2$ with different Zn contents is shown in Fig. 8C, it is found that the photosensitized degradation activity can be enhanced by doping an appropriate amount of Zn. Among these, sample B (Zn doping content is 0.37%) shows the highest activity. After irradiation for 30 min, the degradation rates for sample B and sample A (pure anatase $TiO_2$ sample) are 99.4% and 63.5%, respectively. The time required for the complete degradation of RhB is about 30 min for sample B, while 75 min for sample A. And the photosensitized degradation activity of RhB is decreased gradually with increasing Zn content.

### 3.3. Photocatalytic mechanism

The photosensitization degradation reaction can be summarized in the following five steps:

$$\mathrm{dye_{ads}} + h\nu(\lambda > 420\,\mathrm{nm}) \rightarrow \mathrm{dye_{ads}}^{*} \quad \text{(excitation reaction)} \tag{1}$$

$$\mathrm{dye_{ads}}^{*} + \mathrm{TiO_2} \rightarrow \mathrm{dye_{ads}}^{\bullet +} + \mathrm{TiO_2}(\mathrm{e_{cb}}^{-}) \quad \text{(electron injection reaction)} \tag{2}$$

$$\mathrm{dye_{ads}}^{\bullet +} + \mathrm{TiO_2}(\mathrm{e_{cb}}^{-}) \rightarrow \mathrm{dye_{ads}} \quad \text{(charge recombination reaction)} \tag{3}$$

$$TiO_2(e_{cb}^-) + O_2 \rightarrow O_2^{\bullet -} \quad \text{(electron scavenging reaction)} \tag{4}$$

$$dye_{ads}^{\bullet +} + (O_2^{\bullet -} \text{or} {}^{\bullet}OH) \rightarrow \rightarrow \text{degradation} \tag{5}$$

Firstly, the excited dye molecules are generated upon absorption of visible photons and subsequently injecting electrons into $TiO_2$ conduction band. After Zn doping, which presents in the form of small ZnO nuclei and disperses randomly on the anatase $TiO_2$ surface, the charge transfer between $TiO_2$ and RhB is promoted. According to Fig. 9, two main reactions can take place due to suitable energetic positions of RhB and ZnO:

$$dye_{ads}^{\bullet +} + ZnO \rightarrow dye_{ads}^{\bullet +} + ZnO(e_{cb}^-) \tag{6}$$

$$ZnO(e_{cb}^-) \rightarrow TiO_2(e_{cb}^-) \tag{7}$$

These reactions can be described as (i) the electron injection from the excited state of RhB to the conduction band of ZnO (reaction (6)) and (ii) the relaxation process of the hot electron from the conduction band of ZnO to $TiO_2$ (reaction (7)). Thus, electron injection into the conduction band of $TiO_2$ can be enhanced by the synergistic capture of electron reaction due to the presence of ZnO on the anatase $TiO_2$ surface. The injected electron reacts with the surface-absorbed $O_2$ to yield active oxygen radicals (e.g., $O_2^{\bullet -}$, $^{\bullet}OOH$, $^{\bullet}OH$). Subsequently, the dyes are degraded or mineralized by these oxygen radicals. Therefore, the resultant RhB degradation rate is enhanced.

The amount of Zn dopants also plays an important role in determining the photocatalytic activity of $TiO_2$ nanoparticles. XPS results prove that the percentage of surface oxygen vacancies is increased with increasing Zn doping content. The surface oxygen vacancies of $TiO_2$ can induce sub-band levels near the bottom of the conduction band (Fig. 9) and easily capture photoinduced electrons [30]. It was reported that the photoexcited electron, captured by sub-bands related to oxygen vacancies could enhance the separation of photoexcited chargers, resulting in the improvement of the photocatalytic activity of $TiO_2$ under UV irradiation [23]. According to the $TiO_2$-assisted photosensitized degradation process, the surface oxygen vacancies of $TiO_2$ can be considered as electron traps, which would retard both scavenging the injected electron (reaction (4)) and charge recombination reaction (reaction (3)). In RhB-sensitized $TiO_2$ systems, the standard redox potentials of the $O_2/O_2^{\bullet -}$ couple $\{\{EO_2/O_2^{-\bullet} = -0.28\,V\}\}$ is more positive than $RhB/RhB^{\bullet +}$ couple $\{E_{RhB/RhB^{\bullet +}} = -1.09\,V\}$ (Fig. 9) [34]. This means that the driving force for charge recombination reaction is much higher than that of the electron scavenging reaction. So the injected electron scavenging reaction should be the rate-determining step. The net effect of the excessive surface oxygen vacancies would retard the electron scavenging reaction more preferentially than the charge recombination reaction. Consequently, the expected dye degradation activity could be reduced when forming excessive surface oxygen vacancies of $TiO_2$ by higher Zn doping.

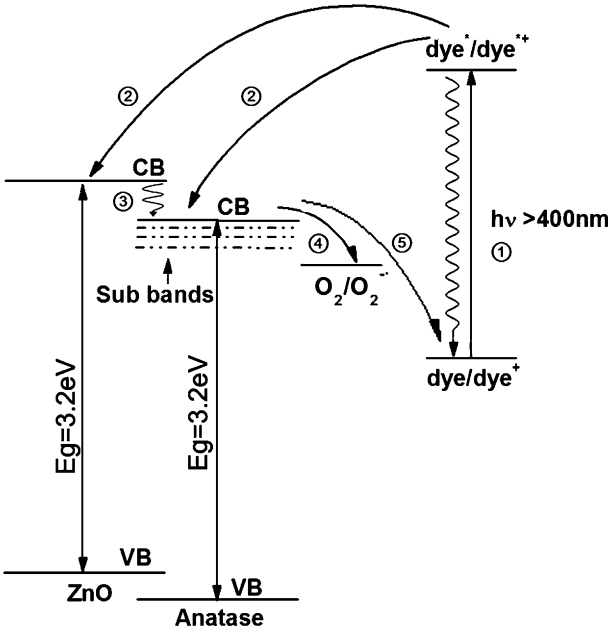


Fig. 9. Schematic illustrating the electron transfer pathway for the photodegradation of RhB on Zn-doped $TiO_2$ under visible irradiation. The numbers represent main elementary paths: (1) dye excitation by visible light; (2) electron injection from the excited dye into the CB of $TiO_2$ or ZnO; (3) the hot electron relaxation from the conduction band of ZnO to $TiO_2$; (4) yield active oxygen radicals; (5) back-transfer of electrons to the oxidized dye.

## 4. Conclusions

Zn-doped $TiO_2$ nanoparticles with high photocatalytic activity were successfully synthesized through the diffusion flame method. Optimum content of Zn doping $TiO_2$ sample (0.37% Zn) would result in the improvement of photosensitized RhB dye-degradation activity under visible light irradiation. The increase in activity has been attributed to suitable energetic positions between ZnO formed on $TiO_2$ particles surface and the excited state of the dye, which enhanced the electron injection into the conduction band of $TiO_2$ by capturing electron reaction of ZnO. However, more doping would lead to the formation of excessive surface oxygen vacancies, which would act as electron traps and retard electron transfer process, thereby undermining the photocatalytic activities. The experimental results demonstrate that the $TiO_2$ nanoparticle with optimal Zn doping can be considered a promising photocatalyst in the photosensitized degradation of dyes under visible light irradiation.

## Acknowledgments

This work was supported by the National High Technology Research and Development Program of China (2006AA03Z358), the National Natural Science Foundation of China (20236020, 20706015), the Shanghai Municipal Science and Technology Commission (06DZ05902, 05DZ22302 and 045211021), Special Project for Nanotechnology Shanghai (0452nm001, 0452nm047, 0752nm010 and 0552nm001), Shanghai Rising-Star Program (06QA14013) and 973 program (2004CB719500). Dr. Du's international travel was funded by the Royal Society, UK.

## References


[1] D.F. Olis, E. Pelizzetti, N. Serpone, Environ. Sci. Technol. 25 (1991) 1523.
[2] J.R. Bolton, Sol. Energ. Mater. Sol. Cells 38 (1995) 543.
[3] S. Sodergren, A. Hagfeldt, J. Olsson, S.E. Lindquist, J. Phys. Chem. 98 (1994) 5552.
[4] C. Kormann, D.W. Bahnemann, M.R. Hoffmann, J. Phys. Chem. 92 (1988) 5196.
[5] M.A. Fox, M.T. Dulay, Chem. Rev. 93 (1993) 341.
[6] R. Asahi, T. Morikawa, T. Ohwaki, K. Aoki, Y. Taga, Science 293 (2001) 269.
[7] H. Gerischer, A. Heller, J. Phys. Chem. 95 (1991) 5161.
[8] B. Ohtani, K. Iwai, S. Nishimoto, S. Sato, J. Phys. Chem. B 101 (1997) 3349.
[9] K. Wu, Y. Xie, J. Zhao, H. Hidaka, J. Mol. Catal. 144 (1999) 77.
[10] C. Galinado, P. Jacques, A. Kalt, Chemosphere 45 (2001) 997.
[11] C. Chen, W. Zhao, J. Li, J. Zhao, Environ. Sci. Technol. 36 (2002) 3604.
[12] H.M. Sung-Suh, J.R. Choi, H.J. Hah, S.M. Koo, Y.C. Bae, J. Photochem. Photobiol. A 163 (2004) 37.
[13] T. Wu, G. Liu, J. Zhao, H. Hidaka, N. Sperpone, J. Phys. Chem. B 102 (1998) 5845.
[14] C. Chen, X. Li, W. Ma, J. Zhao, J. Phys. Chem. B 106 (2002) 318.
[15] Y.M. Gao, W. Lee, R. Kershav, K. Dwight, S. Wold, Mater. Res. Bull. 26 (1991) 1247.
[16] N. San, A. Hatipoglu, G. Kocturk, Z. Cmar, J. Photochem. Photobiol. A: Chem. 146 (2002) 189.
[17] U. Siemon, D. Bahnemann, J.J. Testa, D. Rodriguez, M.I. Litter, N. Bruno, J. Photochem. Photobiol. A: Chem. 148 (2002) 247.
[18] J. Zhu, W. Zheng, B. He, J.L. Zhang, M. Anpo, J. Mol. Catal. A: Chem. 216 (2004) 35.
[19] G. Marci, V. Augugliaro, M.J. Munoz, J. Phys. Chem. B 105 (2001) 1033.
[20] S.J. Stewart, M.F. Garcia, C. Belver, B.S. Mun, F.G. Requejo, J. Phys. Chem. 110 (2006) 16482.
[21] J. Mair, P. Nair, F. Mizukami, Y. Oosawa, T. Okubo, Mater. Res. Bull. 34 (1999) 1275.
[22] R. Janes, L.J. Knightley, C.J. Harding, Dyes Pigments 62 (2004) 199.
[23] L.Q. Jing, B.F. Xin, F.L. Yuan, L.P. Xue, B.Q. Wang, H.G. Fu, J. Phys. Chem. 110 (2006) 18960.
[24] L. Jing, B. Xin, F. Yuan, L. Xue, B. Wang, H. Fu, J. Phys. Chem. 110 (2006) 17860.
[25] G. Skandan, Y.J. Chen, N. Glumac, B.H. Kear, Nanostruct. Mater. 11 (1999) 149.
[26] H. Wang, in: Proceedings of the Fall Meeting of Eastern States Section of the Combustion Institute, Pennsylvania State University, University Park, PA, October 26–29, 2003.
[27] Y. Zhao, C.Z. Li, X.H. Liu, et al. Mater. Lett. 61 (2007) 79.
[28] Y. Zhao, C.Z. Li, X.H. Liu, F. Gu, J. Alloy. Compd. 440 (2007) 281.
[29] R. Sanjines, H. Tang, H. Berger, F. Gozzo, G. Margaritondo, J. Appl. Phys. 75 (1994) 2945.
[30] L.Q. Jing, Z.L. Xu, X.J. Sun, W.M. Cai, Appl. Surf. Sci. 180 (2001) 308.
[31] J.G. Yu, H.G. Yu, B. Cheng, X.J. Zhao, J.C. Yu, W.K. Ho, J. Phys. Chem. B 107 (2003) 13871.
[32] Y. Wang, N. Herron, J. Phys. Chem. 95 (1991) 525.
[33] L.Q. Jing, X.J. Sun, J. Shang, W.M. Cai, Z.L. Xu, Y.G. Du, H.G. Fu, Sol. Energ. Mater. Sol. Cells 79 (2003) 133.
[34] H. Park, W. Choi, J. Phys. Chem. B 109 (2005) 11667.